Characterization of blocks within a near seafloor Neogene MTC, Orange Basin: Constraints from a high-resolution 3D seismic data

Paschal Ogechukwu Amaechi [a,*], Nicolas David Waldmann [b], Yizhaq Makovsky [b], Mimonitu Opuwari [a]

[a] Petroleum Geology Research Group, Department of Earth Sciences, University of the Western Cape, 7535 Bellville, South Africa
[b] Dr. Moses Strauss Department of Marine Geosciences, University of Haifa, 3498838 Mt. Carmel, Israel

ARTICLE INFO

ABSTRACT

Submarine mass wasting processes in deepwater settings can incorporate large blocks, which may play a key role in deepwater geological processes and geohazard assessment. However, there is a limited understanding of the deformation style arising from the interaction between submarine blocks and structural/bathymetric barriers such as ramps. The deformation and kinematic history of several submarine blocks (with a thickness of up to 150 m) within a near seafloor mass transport complex in the Orange Basin are documented using seismic geo-morphic methods. The interpreted blocks are preserved in three discrete fault-bounded morphological terrains within a Neogene mass-transport complex. These terrains vary in lengths from 2 km to 6 km; they have heights of 60 m to 150 m and are characterized by discrete and localized structural highs on the present-day seafloor. Block sizes vary across terrains suggesting differences in the block evolution process. Blocks near the ramp appear in seismic profiles comprising (a) Chaotic and transparent seismic reflections and (b) parallel to sub-parallel, continuous, low to moderate amplitude reflections. This variability in seismic facies of the blocks reflects the de-gree of their interaction and translation over a ramp at the basal shear zone of the mass transport complex, ev-idenced by the difference in the block features on the upslope portion of the ramp versus the downslope part. Notably, the deformation styles recorded in the blocks show the impact of the ramp during mass flow, which has broader implications for understanding the internal mechanisms of blocky mass transport complexes in many continental margins.

1. Introduction

Mass transport complexes (MTC) are by-products of underwater mass-wasting processes, which contribute considerably to basin infill, basin morphology, and the producibility of deepwater petroleum systems (e.g., Alves, 2015; Cox et al., 2020). MTCs comprise several gravity-induced deposits that move downslope on a basal shear surface or basal shear zone (BSS), occurring in subaerial and submarine environments (Moscardelli et al., 2006). Other than gravity, rapid sedimentation, earthquakes, tsunamis, oversteepening of slopes, gas escape, changes in the hydrodynamics conditions, any other factor that results in sediment or sedimentary rock failure can induce submarine mass wasting process (Gee et al., 2006; Masson et al., 2006; Zitter et al., 2012; Urlaub et al., 2013; Urgeles and Camerlenghi, 2013). Based on the degree of internal cohesiveness, a failed stratigraphic package can be divided into submarine slides, slumps, and debris flows (Pickering and Corregidor, 2005; Shanmugam, 2015; Scarselli et al., 2016). The

rapidness and downward flow of turbidites due to turbidity current are similar to the flow nature of mass transport complexes. Mass wasting processes have been closely linked to turbidity currents by various authors (e.g., Dott Jr., 1963; Gee et al., 2001; Shanmugam, 2013; Mosher et al., 2017). Often, mass transport complexes include coherent strata known as block features (Gamboa et al., 2011).

Several studies have documented the occurrence of MTCs along continental margins (Garziglia et al., 2008; Giles et al., 2010; Cossey, 2011; Ogiesoba and Hammes, 2012; Strasser et al., 2012; Deckers, 2015; Shipp et al., 2015; Moore and Strasser, 2016; Rusconi, 2017), with the presence of internal blocky features (Davis et al., 1979; Nissen et al., 1999; De Blasio et al., 2006; Locat et al., 2010; Alves, 2015; Sobiesiak et al., 2016; Ward et al., 2018; Cox et al., 2020; Sobiesiak et al., 2020; Wu et al., 2021). Our study interprets a near seafloor MTC containing blocks in the Orange basin, offshore South Africa using high-resolution 3D seismic data. The recognition of blocks in seismic data depends on the internal reflection architecture of MTCs (Steventon et al., 2019; Nugraha et al., 2020). The recognition and interpretation of blocks within mass transport complexes throw up several geologic and geohazard implications (Hodgson et al., 2018; Artoni et al., 2019).

* Corresponding author.
E-mail address: pamaechi26@gmail.com (P.O. Amaechi).

Blocks have been documented to have several impacts on underwater communication installations and oil-gas platforms (Deptuck et al., 2007; Vanneste et al., 2013; DeVore and Sawyer, 2016).

Geological successions with deformed and undeformed blocks have been shown to offer potential hydrocarbon sources (Wendorff, 2003; Ogiesoba and Hammes, 2012; Bhattacharya et al., 2020). This is based on the fact that MTCs shape the bathymetry of the submarine environment and define the re-routing of deep water sediment transport systems, such as turbidite channels (Crespo-Blanc and Campos, 2001; Peel, 2014; Dalton et al., 2017; Nwoko et al., 2020). MTCs consisting of a coherent seismic stratigraphy tend to ramp up in their contractional domain (Gawthorpe and Clemmey, 1985; Trincardi and Argnani, 1990; Strachan, 2002; Lucente and Pini, 2003; Martinez et al., 2005; Bull et al., 2009). Ramps are described as a segment of basal shear surface that truncates bedding planes of a stratigraphic section depicting a localized variation of stress and failure conditions (Alves, 2015). The variations of stress and failure during the translation of MTCs ultimately result in the formation of blocks or megaclasts (Nugraha et al., 2020). An MTC whose translation is inhibited by a ramp is described as a frontally confined MTC, while an MTC, which translates over a ramp and over the contemporaneous seafloor, is described as a frontally emergent MTC (Martínez et al., 2006; Moernaut and De Batist, 2011). The trend of a ramp with other indicators indicates the translation direction of the MTC and subsequent deformation of the block (Bull et al., 2009).

Our study presents an interpretation of high-resolution 3D seismic data that includes buried submarine blocks associated with a seafloor MTC in the Northern Orange Basin, offshore South Africa (Fig. 1). In addition, we also examine the impact of block translation on creating features such as scours and other erosional morphologies at the base of the MTC. However, an increase in our understanding of the nature of the interaction between ramps and blocks contained within the MTC is needed. This understanding will have broader implications for retracing the structural evolution of the Orange basin, predicting the possible reactivation of MTC processes in the Orange basin and other passive margins around the world.

2. Geological setting

The Orange Basin, a Southwest African Coastal basin stretching between Namibia and South Africa, covers an area of about 160.000 km^2, and it is adjudged the largest offshore basin extending from the territorial waters of Namibia to South Africa (Hirsch et al., 2007; Isiaka et al., 2017). As a passive volcanic margin, the Orange Basin was characterized by several subsidence episodes that lasted approximately 10 Ma (Muntingh and Brown Jr., 1993).

Stratigraphically, the formation stage of the Orange Basin can be divided into three units: pre-rift, *syn*-rift, and post-rift. In the southwestern continental margin of the Orange Basin, the post-rift sediments are underlain by pre-rift and syn-rift grabens (Jungslager, 1999; Kuhlmann et al., 2010; De Vera et al., 2010), while complex gravity-collapse systems deformed the post-rift Cretaceous and Paleogene sediments (Paton et al., 2007; De Vera et al., 2010). The history of the Orange Basin sedimentary infill is summarized as follows (Brown, 1995; Paton et al., 2007): the Orange Basin's major depocenter was filled by a southern fluvial system (the Olifants River) between ~117.5 and 103 Ma (Samakinde et al., 2021). During this period, sediments were also fed into the basin by minor river systems along the Agulhas-Columbine Arch coastlines. The principal depocenter was located 200 km southwest of Alexander Bay, and it evolved in response to the shift in the drainage system of the Olifants River (e.g., Brown, 1995). Moreover, the Orange fluvial and deltaic systems laterally shifted westward, resulting from increased sediment supply and accommodation space (Burgess and Hovius, 1998; Goodbred and Kuehl, 2000; Petroleum Agency of SA, 2008; Carvajal et al., 2009). With the Cretaceous
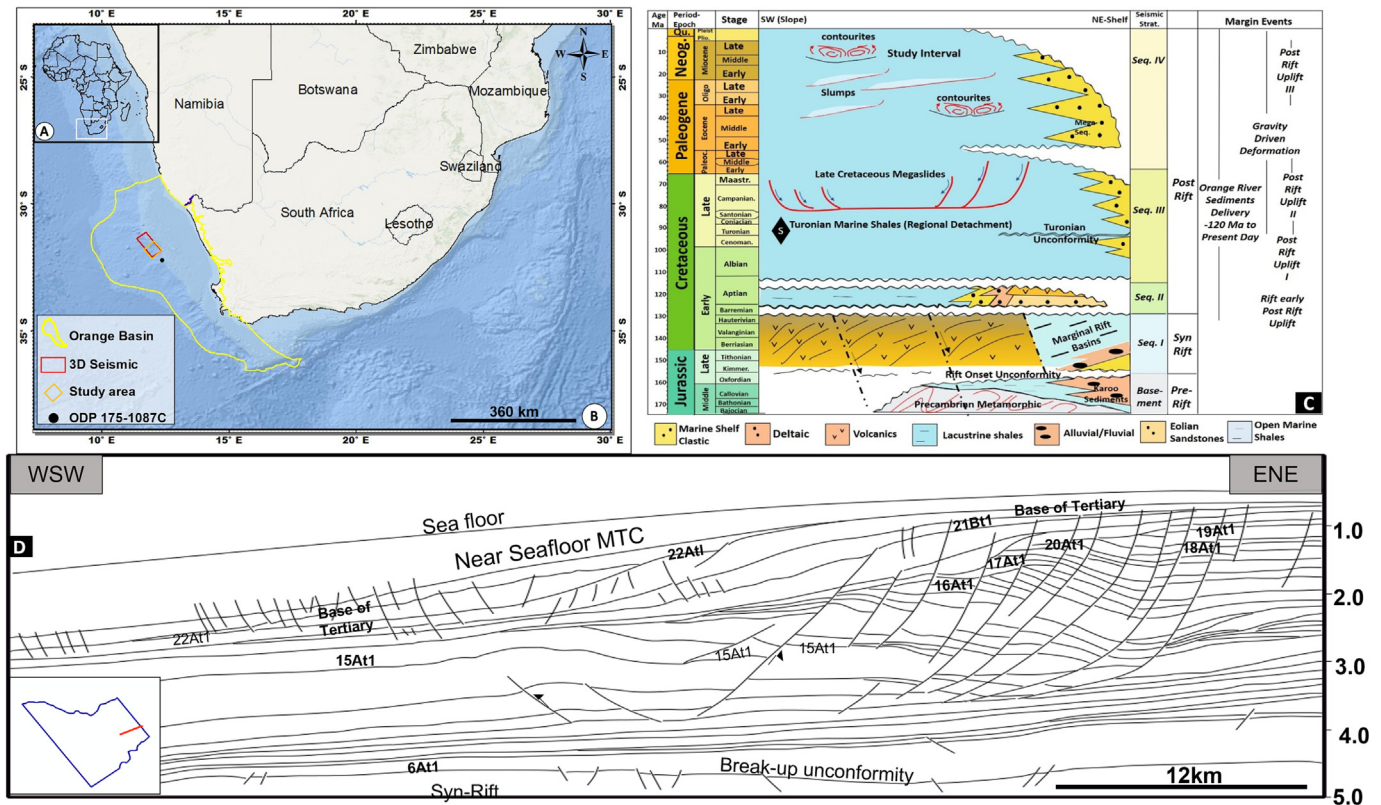

Fig. 1. Location Map of the study area (A) Inset map of Africa showing the location of Southern Africa. (B) Map of southern Africa showing the location of the study area (C) Chrono- and lithostratigraphy of the Orange Basin showing the main geodynamic events and stratigraphy of the study area (Scarselli et al., 2016). The studied MTC belongs to the post-rift Sequence IV of the chronostratigraphic setting of the basin (D). Interpreted seismic reflection profile by (Muntingh and Brown Jr., 1993) showing the sequence stratigraphy of the Orange basin.

sediments becoming stable, the subsidence rate reduced, and the Paleogene depocenter shifted basinward. This prolonged stacking of the Paleogene deposits on the continental slopes resulted in gravity-driven faulting at the shelf's edge and was coeval with sedimentation (De Vera et al., 2010; Hirsch et al., 2010).

3. Data and methods

The data used in this study is a high-quality 3D seismic reflection survey covering approximately 8200 km^2 of the Orange Basin. The 3D seismic data was acquired using the M/V Polar Duchess in a Shell SA OB12 project from the 25th of October 2012 to the 22nd of February 2013. The seismic data has a line spacing of 25 m. A nominal common midpoint (CMP) of 80-fold was used to ensure high-resolution images. A sampling rate of 2 ms was adopted in the data acquisition.

The 3D seismic data was loaded into the seismic interpretation software Petrel 2019. Before seismic interpretation, structural smoothing was carried out, which is necessary to reduce the number of artefacts, maintain the sharpness of the detected edges, and improve the initial seismic interpretation, especially in heavily deformed areas. The structural smoothing attribute involves applying a spatial filter that removes noise from seismic data while preserving critical geometric characteristics and discontinuities (Ngeri et al., 2015; Omosanya et al., 2020). The filter size controls the number of traces horizontally and vertically.

Two main seismic horizons representing the top (seafloor) and the basal shear surface were mapped using guided auto-tracking and manual corrections. The top of an MTC is defined by a rugged bounding surface located above discontinuous, chaotic, and sometimes heterogeneous amplitude reflections. On the other hand, the basal shear surface (BSS) lies at the base of an MTC and separates it from the underlying continuous and well-stratified reflections.

The MTC's internal features were described with: (a) Seismic facies (SF), which include Blocks separated by faults and distinguished by discontinuous to chaotic reflections with generally flat bottom surfaces and irregular upper surfaces. (b) Chaotic and translucent seismic facies exhibiting a high degree with general flat base surfaces. (c) Seismic facies that is parallel to subparallel, continuous to semi-continuous, and have low to moderate amplitude reflections.

The internal architecture of the MTC was mapped using seismic geomorphological techniques, which involve a detailed correlation of seismic profiles and high-resolution mapping of the tops and bottoms of reflection events or horizons. The interpretations were supported by seismic attribute maps, such as Root Mean Square (RMS), variance, and edge detection attributes. Seismic attributes were calculated using inline and crossline filter lengths of a mild smoothening range of 8 to 15 samples (Chopra and Marfurt, 2008). The computed variance and edge detection attribute enhanced the outline and visualization of faults and block edges within the MTC. Variations in reflection due to lithology changes, sedimentation patterns, grain size, and compaction effects were highlighted using the root mean square (RMS) (Koson et al., 2014; Gamboa et al., 2020). In addition, several variance slices were extracted to show internal structural components, further corroborated by the seismic profiles. For example, blocks with coherent reflections identified in seismic profiles were validated with the undisturbed areas on the variance slices, while discontinuities and faults were interpreted as high variance coefficients.

Morphometric analysis involving the measurement of height (block thickness), width (short block axis), and length (long block axis) were carried out using the ruler tool on 2D profile sections as well as on the 3D window of the Petrel software. The shape of the blocks was estimated using the folk and Sneed tri-plot template. Description of the measured parameters using scatter plots of the width, height, and length allowed us to understand the morphological and morphometric character of the blocks and their relationship with the underlying basal ramp. The length was measured as the long axis of the block. The width/length cross-plot was used to assess the blocks' elongated and concentric nature. Block height is usually limited by or related to the thickness of the MTC (Gamboa et al., 2011). Correlation coefficients provided insights into how the different block parameters associate with each other.

4. Results and interpretation

4.1. Seismic geomorphology of the mass-transport complex

The MTC area is divided into three seismic units (Fig. 2) based on seismic facies recognition studies by (Prather et al., 1998). The Neogene MTC mapped in this study area is about 60 km long and 85 km wide on an SW-NE axis. The MTC is bounded at the base by a basal shear surface (BSS), and the top corresponds to the seafloor reflection. Slope gradient and ramp development can be noticed in several sections of the BSS. The
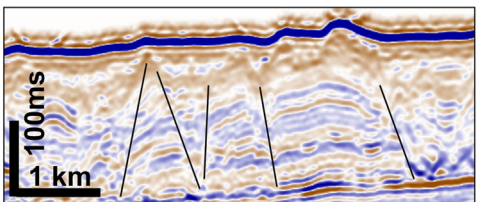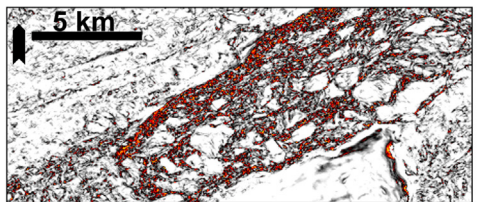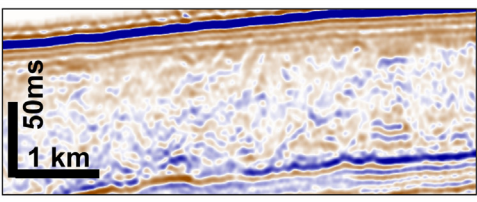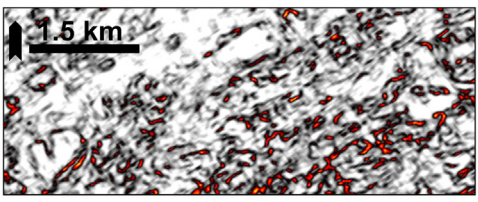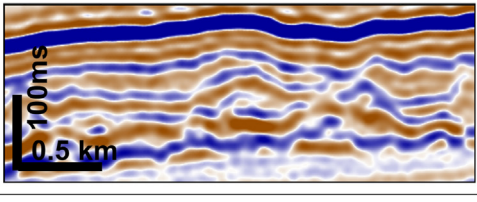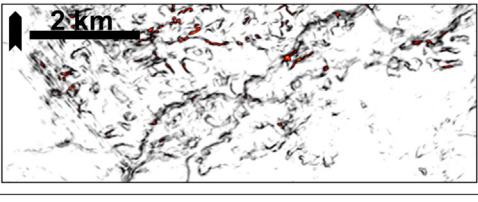
Seismic Section	Variance Slice	Description
		Blocks separated by faults and characterized by discontinuous to chaotic low amplitude reflections with generally flat basal surfaces and irregular upper surface.
		Chaotic and transparent facie Showing complete deformation. Generally, with flat basal surfaces.
		Parallel to sub parallel, continuous to semi-continuous facies with low to moderate amplitude reflections

Fig. 2. Seismic facies (SF) observed in the study area: SF 1 and 2 make up the slide and the blocks in the study area, while SF3 essentially makes up the undeformed areas.
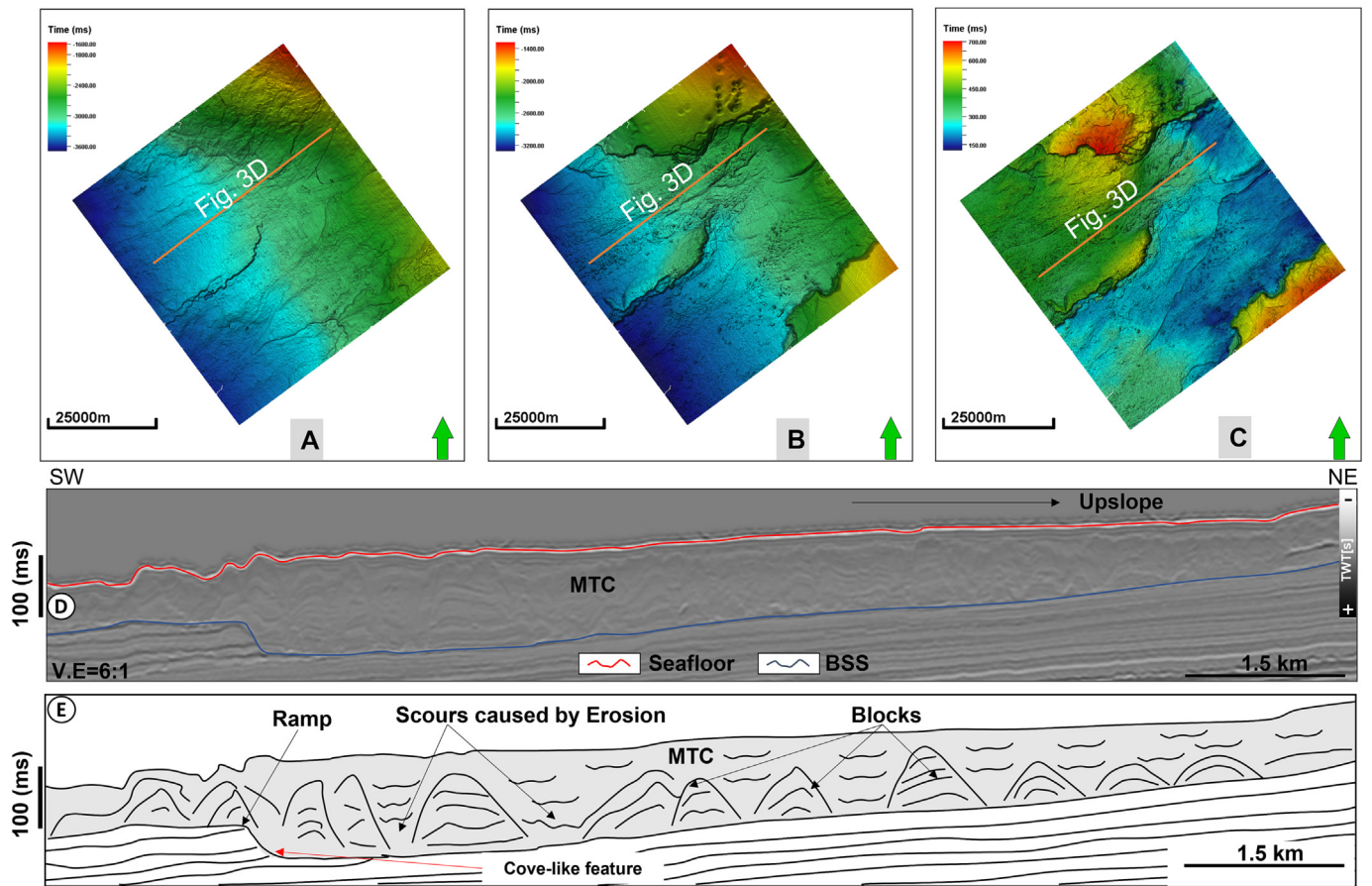
Fig. 3. Structural maps of the (A) Basal shear surface of the MTC (B) Top surface of the MTC and (C) Thickness map between the top and the base MTC (D) Uninterpreted seismic profile of the MTC (E) line drawing interpretation of the seismic profile showing major features of the MMTC.

interpreted MTC is characterized as a blocky MTC (Ward et al., 2018; Kumar et al., 2021), and the blocks within the MTC are strongly associated with substrate tooling or ploughing (Kumar et al., 2021). Features like the cove-like structure and grooves associated with the interpreted ramp provided evidence of erosion during the translation of the MTC (Fig. 3).

Although MTCs are typically divided into headwall, translational and toe domains (Prior et al., 1984; Martinez et al., 2005; Bull et al., 2009), these geomorphological parts of the interpreted MTCs were not imaged by the 3D seismic data coverage as the survey was acquired about 240 km away from the shelf. However, the source area of the MTC is inferred to be located upslope to the NE (Fig. 3). Similarly, the data coverage did not allow for a definitive classification of the MTC as detached or attached according to the classification system of (Moscardelli and Wood, 2008), but relying on previous work in the study area (Brown, 1995; Dalton et al., 2017) we project that the MTC is attached to the shelf in the NE direction. The BSS of the MTC appears as a continuous high amplitude reflection, dipping to the SW, on a slope that ranges between 0.15° and 0.22° and with relief between 1830 m to about 2500 m.

Fig. 4 further highlights the erosional morphologies found within the MTC, including striations and grooves that likely resulted from block movements. These morphological features are also kinematic indicators for erosional activities (Sobiesiak et al., 2018). Striations and grooves were dominant features in the central part of the MTC and are generally trending to the southwest. The striations are up to 2 km long, while the groove measures up to 15 km and can be found on the BSS to a depth of about 3000 m. Furthermore, the observed striations are remarkably parallel and do not show significant downslope divergence. Hence, the general NE-SW orientation of the grooves and striations points to a SW

direction of mass transport for the MTC. In addition to the observed erosional indicators, a NE-SW trending cove-like depression is also interpreted on the BSS of the MTC (Fig. 5). This depression is ~19 km long and has a width of ~7 km and a depth of 250 ms. The MTC is divided into three zones (Fig. 4) according to the concentration of the blocks and to highlight kinematic features. The zones were also delineated based on the intensity of the erosional activities—zone 1 comprising the downslope blocks with visible striations. Zone 2 comprises blocks close to the ramp; erosional features like grooves or coves are observed here, suggesting high erosion intensity. Lastly, the zone 3 area contains blocks not associated with the ramp. The near absence of erosional features suggests waning erosional intensity. A significant basal ramp (Fig. 3), spanning about 27 km, dipping to the NE and with a maximum height of about 300 m, is located at the central part of the MTC with an average inclined angle of 1.5° to the NE direction.

4.1.1. Ramps interpreted within MTC interval

In addition to the MTC's described internal character and geometry, two major kinds of ramps were also interpreted (the down-stepping and the up-stepping ramps). Time-dip, coherence, and RMS amplitude maps of the basal shear surfaces were used to describe the trend and type of ramps. Ramps were described to include structures on the basal shear surface over which a sizable volume of sediment carried across various stratigraphic layers was regarded as ramps (Bull et al., 2009; Martinez et al., 2005). There are several ramps between the MTC's NE- SW trend direction. Among these, two conspicuous ramps located in the southern portion of the study area were interpreted (Fig. 6). The first is an up-stepping ramp (approximately 300 m high) with sediment translation spanning about 25 km in the southwest direction. A second down-stepping ramp (approx. 100 m high), just at the upslope
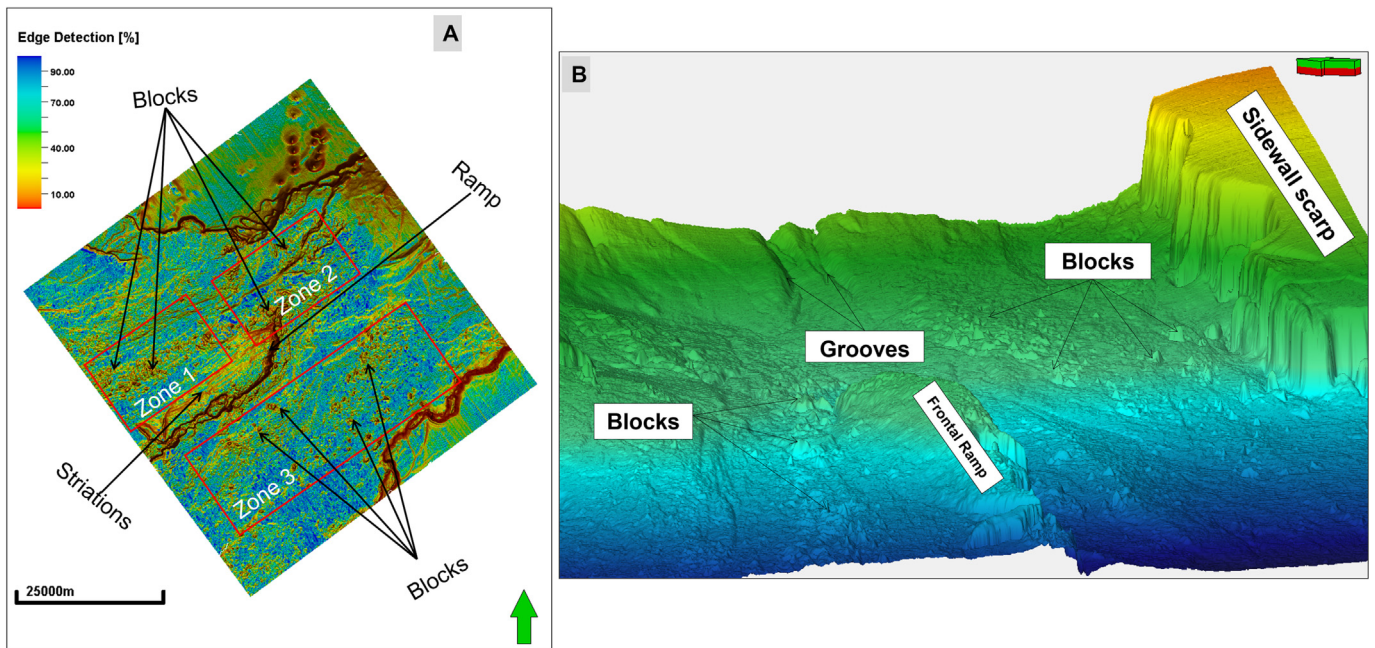
Fig. 4. (A) Edge detection extraction on the MTC top highlighting blocks and striations. Red triangles show the delineated zones of block occurrence in the study area. (B) Three-dimensional perspective view of the MTC top surface showing seafloor expression of blocks, grooves, and scarp features.

Fig. 5. Geomorphologic features associated with the BSS of the MTC (A) A time-migrated structure map of the Basal surface showing kinematic features such as scours, grooves, scarps, and ramps (B) zoomed-in section showing erosional features like cove and striations identified on the BSS. The striations are oriented in the NE-SW direction depicting the SW direction of mass transport. (C) A zoomed-in section shows the scours.

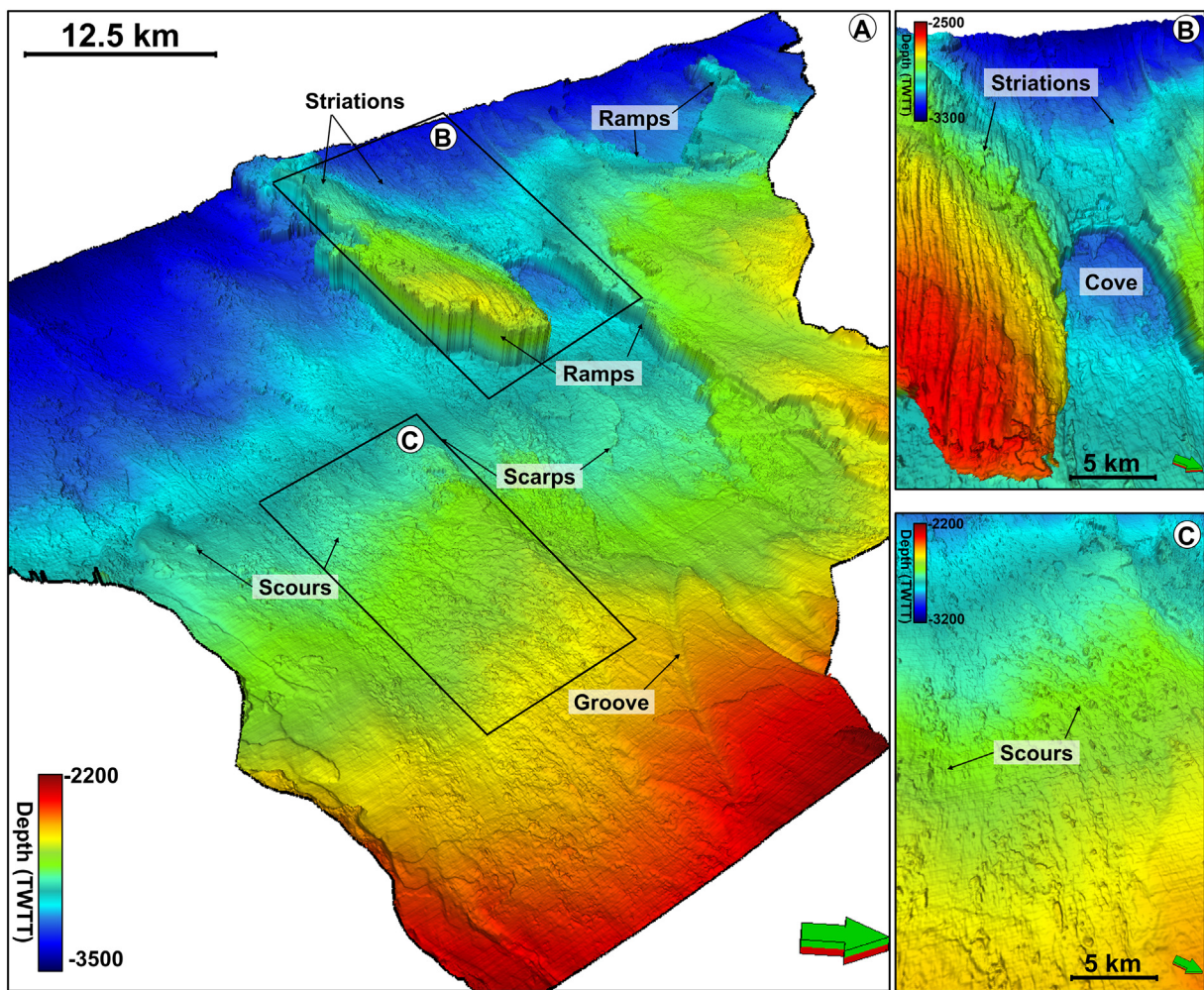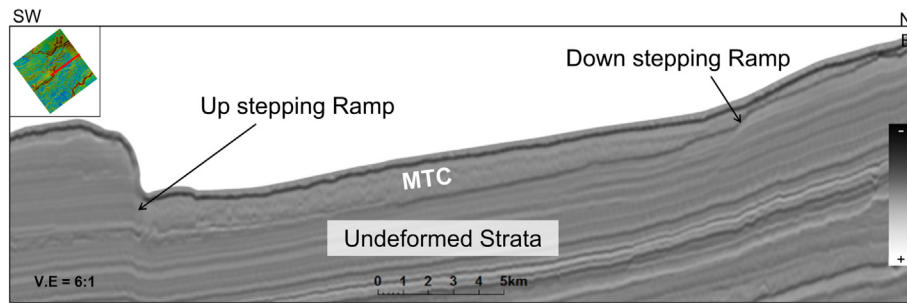**Fig. 6.** Seismic profile through the MTC showing a down-stepping ramp towards the NE and an up-stepping ramp towards the SW. An interpreted horizon within the undeformed strata in the area reveals the slope gradient variations, which may have contributed to the development of the ramp.

region of the MTC, sets the stage for the Southwest translation direction of the MTC. Structural features like scarps, erosional scours, and promontory-related highs characterize the gradient changes of the two ramps. However, ramp two tend to be more fault controlled with the presence of an underlying fault.

4.2. Internal architecture of submarine blocks

Submarine blocks within the MTC are characterized by high amplitude reflections, which contrast with the chaotic and low amplitude reflections of the MTC. Interpreted blocks exhibit varying attributes (ranging from sizes, orientations, and seismic facies) in their internal architecture (Gamboa et al., 2012). Generally, the blocks are separated by faults (Fig. 2), with their internal fabric sometimes exhibiting chaotic and tilted reflections. Blocks in the central part of the MTC showed long axes, with orientations, heights, and sizes sometimes varying locally in relation to the basal ramp. In the distal portion of the MTC (Corresponding to zone 3), submarine blocks are sparse (with about ten blocks identified), with an average size of 109 m. Conversely, in the proximal to the downslope portion of the MTC (Corresponding to zones 1 and 2, with about 31 blocks analyzed), blocks become thicker (With an average size of 183 m) and are sometimes exposed at the seafloor. The blocks then become more detached and deformed after the

ramp towards the SW portion of the MTC (With an average size of 125 m). The seismic facies analysis allowed us to categorize the blocks into minor (300–411 m), moderate (with a size range of 170–260 m), and major deformed blocks (30–130 m) (Fig. 7).

4.3. Morphometry of blocks

The blocks' density within the survey area appears to vary among the three zones (Fig. 8). There are 17 blocks interpreted in zone 2 (with an average block size: of 183 m) and only 10 and 14 for zones 1 and 3 (with Average block sizes: of 125 m and 109 m), respectively. In terms of their area coverage, blocks within the MTC occupy about 23 % (104 km^2) of the total area of zone 1, 34 % (298 km^2) of zone 2, and 1.5 % (13 km^2) of zone 3. The thickest blocks reaching up to 200 m in height and a large surface area of about 137 km^2 are found in zone 2. Average block sizes in zones 1, 2, and 3 are 125 m, 183 m, and 109 m. Similarly, the average height of the blocks falls between 100 m to 200 m, while width and length are variable across the three zones. For example, blocks in zone 1 have the highest length between 1000 m and 1800 m but with slight variations in their width. In zone 2, the blocks have a length of 620 m to 1020 m and a width of 215 m to 465 m, while blocks in zone 3 have lengths and widths of 273 m to 303 m, 355 m, and 1139 m, respectively.
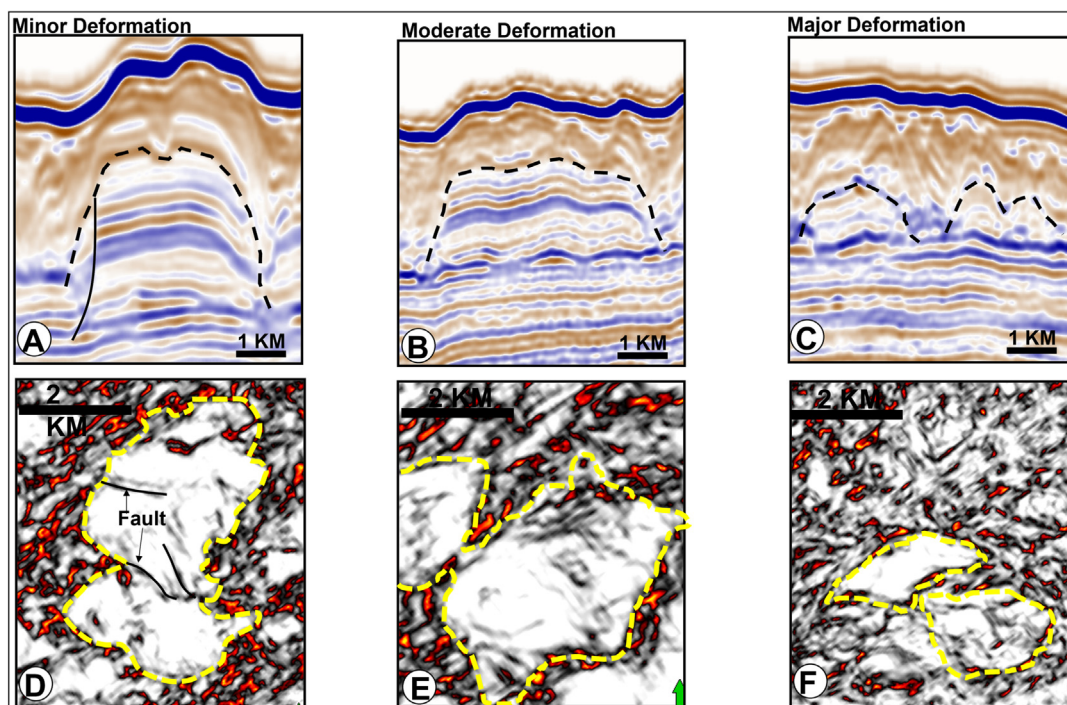
Fig. 7. Different styles of block deformation (A) Minor deformation represented by sub-horizontal internal strata within fault-bounded blocks. (B) Moderately deformed blocks with folding. (C) Major deformation.
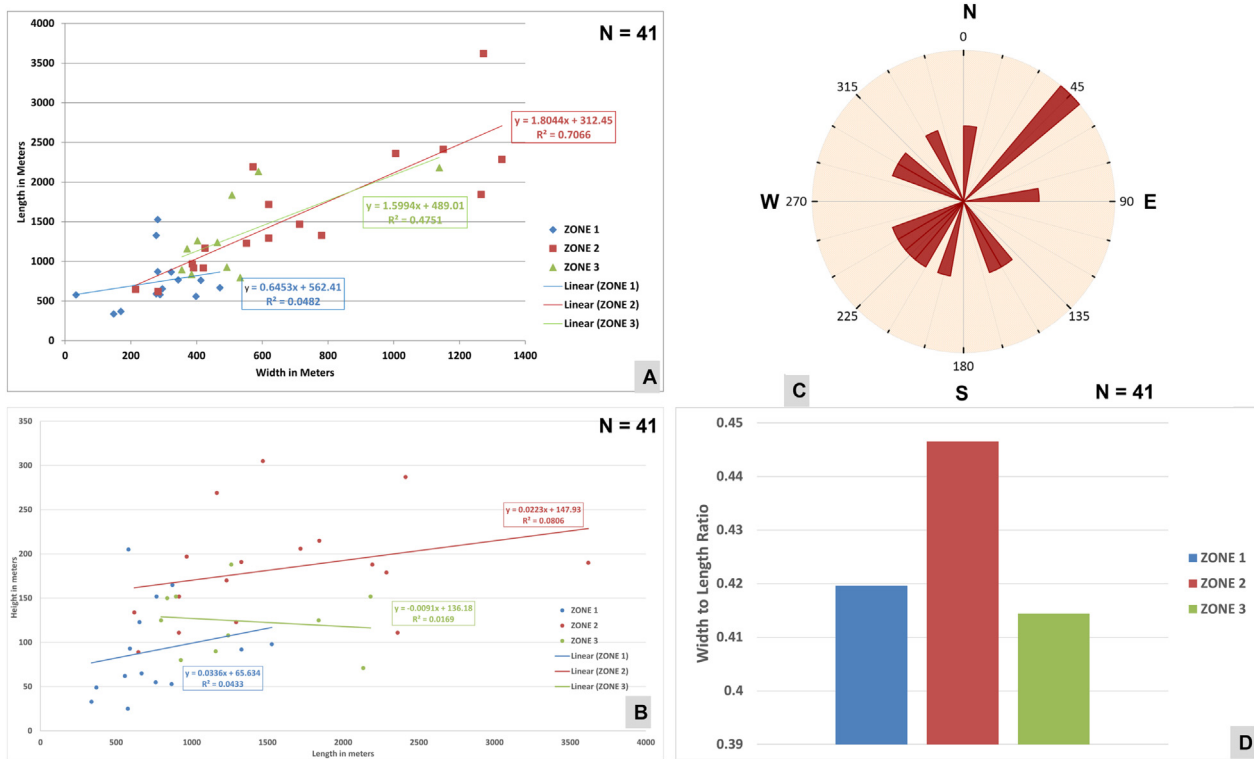
Fig. 8. Visualization and statistical analyses of submarine slide blocks across the three main zones in the study area. (A) Scatter plots of the length vs width across the three zones showing linear regression (B) Scatter plots of the Height vs. Length Vs width across the three zones showing linear regression (C) Rose diagram showing the orientation of the log axes of the locks. The orientation ranges from NE to SW (D) Average width/length ratios for interpreted blocks in the three zones.

Although block size varies across the three zones, their forms do not significantly change. From the proximal to the distal part of the MTC, there is a gradual increase in the block sizes, and just before the ramp, block sizes appear diminished even after the frontal ramp in Fig. 6. Scatter plots of the length and width of the blocks across the three zones yielded a strong coefficient of correlation of R = 0.7066 for zone 2. Also, zones 1 and 3 show a moderately weaker correlation of R = 0.4751 and R = 0.4822, respectively (Fig. 8). The scatter plots of the height and length of the blocks across the zones show weak or no correlation. Hence, we interpreted the positive coefficient of correlations on plots of the length and width of the blocks to indicate that the blocks' width increases and, in some cases, decreases together with the length.

According to (Sneed and Folk, 1958) particle size classification, Blocks within zones 1, 2, and 3 are made up 20 %, 41 %, and 60 % of Very elongated blocks, respectively (Fig. 9). In zone 1 and 2, 23 % and 59 % of the blocks are very bladed, while 14 % of the blocks in zone 1 are very platy.

5. Discussion

5.1. On the origin and features of submarine blocks

Detailed analysis of the internal architecture of the MTC (Figs. 2, 3, and 7) provides valuable information on the heterogeneity of the morphology and internal elements, while analysis of the block deformation (Figs. 7–9) helps understand the provenance of the blocks. The seismic attribute analysis allowed the recognition of different block morphologies in the MTC Blocks exhibited tilted and folded internal seismic reflections revealing their degree of internal deformation, translation, and mass disaggregation. Based on associated features like striations and grooves, blocks are interpreted to have been transported from the NE to the SW of the study area based on their dominant NE SW orientation (Fig. 8C). Some of the blocks appear to be part of the pre-failure strata that survived erosional and mass wasting processes (e.g., Gamboa

et al., 2011; Alves, 2015) and can be described as undeformed sections of the paleo-seafloor usually confined by faults (Fig. 5) and can speak to the blocks travel distance during the mass wasting. The faults separating the blocks MTC point to a synsedimentary deformation. The faulted blocks may further indicate the presence of fluid flow activities in the study area (Hartwig et al., 2012). Hence, the degree of the internal organization of strata within the blocks, the elongated, platy, or bladed nature point to either long or short travel distances or mass disaggregation (Gamboa et al., 2011). Similar to classic siliciclastic transport mechanisms, we propose that blocks with Elongate to blade shapes travelled a long distance before disaggregation, while those with compact to compact platy shapes are suggested to have travelled a shorter distance (Belousov et al., 1999; Haughton et al., 2009).

Sediment source and provenance have often been inferred from information related to variations in the size and shape of sediments (Alves and Cartwright, 2010; Moernaut and De Batist, 2011; Koiter et al., 2013). Omosanya and Alves (2013) conclude that statistical parameters on the geometry of blocks within MTCs could provide reliable information on the provenance, degree of deformation, and depositional processes of submarine blocks. These authors further conclude that the sizes of the blocks in their study area are a function of distance from the source area. In our case, the block sizes in zones 1 to 3 decrease towards the SW, suggesting that the source area of the blocks is located in the NE. Furthermore, the sizes and shapes of blocks can imply different degrees of disaggregation. Larger blocks may have been more mechanically resistant and consequently experienced less disaggregation.

On the other hand, the smaller blocks in zones 1 may have consisted of a large percentage of unconsolidated material and hence travelled longer distances with a higher degree of disaggregation (Hodgson et al., 2018). Moreover, the unconsolidated nature may provide clues on the amount of interstitial water influencing rock mechanics (Jia et al., 2020).

From our statistical analyses, we propose that blocks within zones 1 and 3 with average sizes of 125 m and 109 m and with very elongated
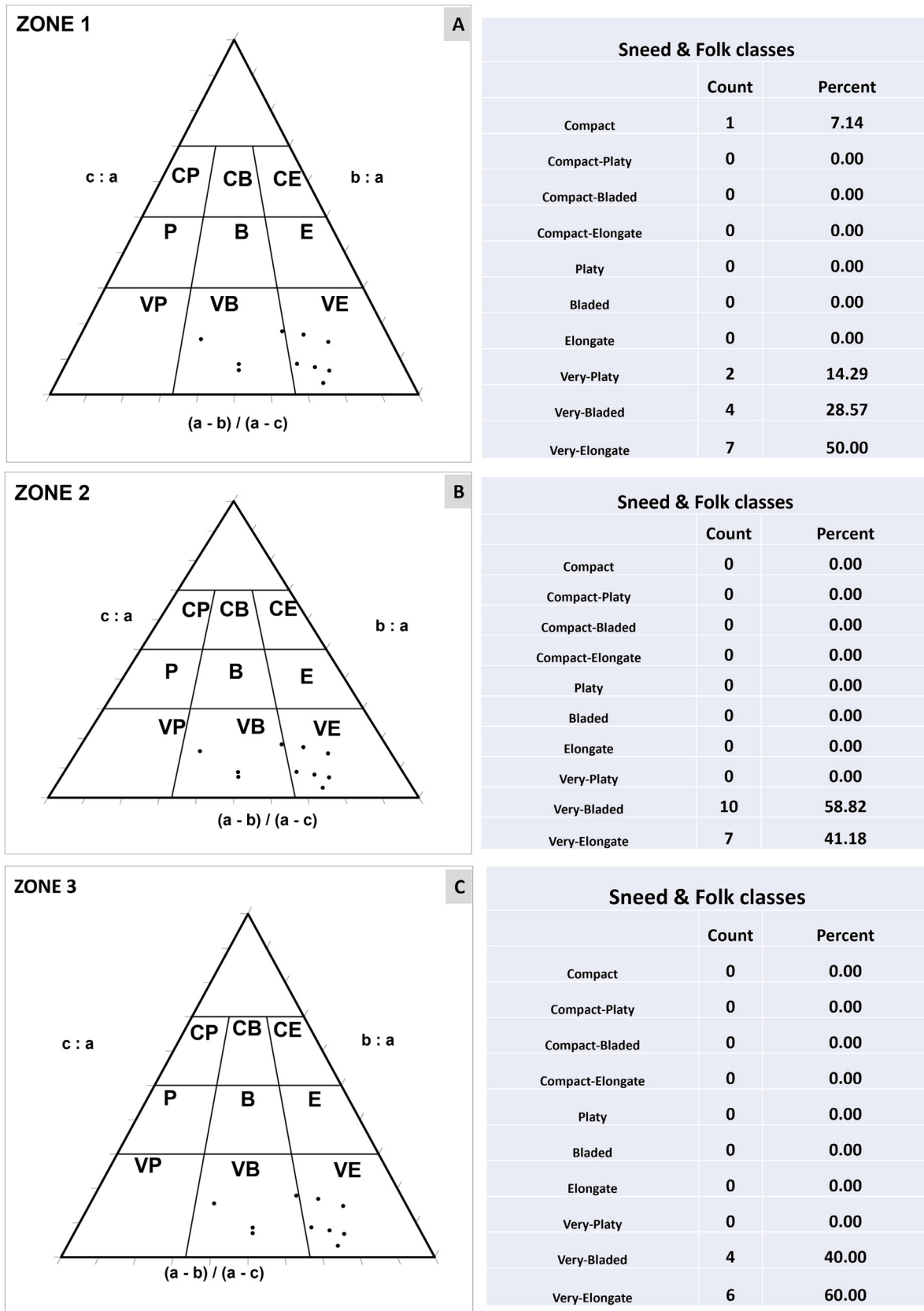
ZONE 1 — A

Sneed & Folk classes		
	Count	Percent
Compact	1	7.14
Compact-Platy	0	0.00
Compact-Bladed	0	0.00
Compact-Elongate	0	0.00
Platy	0	0.00
Bladed	0	0.00
Elongate	0	0.00
Very-Platy	2	14.29
Very-Bladed	4	28.57
Very-Elongate	7	50.00

ZONE 2 — B

Sneed & Folk classes		
	Count	Percent
Compact	0	0.00
Compact-Platy	0	0.00
Compact-Bladed	0	0.00
Compact-Elongate	0	0.00
Platy	0	0.00
Bladed	0	0.00
Elongate	0	0.00
Very-Platy	0	0.00
Very-Bladed	10	58.82
Very-Elongate	7	41.18

ZONE 3 — C

Sneed & Folk classes		
	Count	Percent
Compact	0	0.00
Compact-Platy	0	0.00
Compact-Bladed	0	0.00
Compact-Elongate	0	0.00
Platy	0	0.00
Bladed	0	0.00
Elongate	0	0.00
Very-Platy	0	0.00
Very-Bladed	4	40.00
Very-Elongate	6	60.00

Fig. 9. Fold and sneeds tri-plot for 41 blocks preserved within the seafloor MTC. All the blocks across the three zones mainly plot within the Very-bladed and Very-Elongate shapes. The tri-plot excel template used in this plot was designed by (Graham and Midgley, 2000).

shapes were translated over long distances and thereby experienced a higher degree of disaggregation; In comparison, blocks in zone 2, with an average size of 183 m travelled over shorter distances from their source and thereby experienced lesser degrees of disaggregation. We also propose that the thickness of the slide decreased downslope to the SW as the energy of the slide waned. Scatter plots of the height vs.

length show that block heights decrease with an increase in block lengths in zone 1, and in zone 2, block height decrease with an increase in length, while in zone 3, block heights increase with a decrease in block length (Fig. 7).

5.2. Basal ramp as a control on block deformation

A ramp is a portion of the basal shear surface that cuts across the bedding plane (Trincardi and Argnani, 1990). Ramps are also used to differentiate the mode of emplacement of MTCs, (i.e., frontally confined or frontally emergent MTC). Frontally-confined M.T.C.s undergo a re-stricted downslope translation and do not overrun the un-deformed downslope strata, while frontally-emergent MTCs ramp up from their basal shear zone or surface and translate in an unconfined manner over the ramp (Martínez et al., 2006) as in the case of the study area. Mechanisms surrounding the development of ramps can be attributed to structural obstacles (Trincardi and Argnani, 1990; Moernaut and De Batist, 2011) or coherent stratigraphy within the MTC, which ultimately causes the shear zone to ramp up (Doughty-Jones et al., 2019). More-over, Alves (2015) suggested that seafloor roughness can lead to the generation of ramps. This roughness can be generated by basal tooling or gouging from the translation of blocks, leading to grooves and other erosional morphologies.

Our study interpreted a ramp with varying heights as the MTC shifted southwards, identified towards the SW part of the study area (Fig. 4). The ramp likely developed from a combination of structural and erosional processes with the final morphology principally modulated by erosional processes, as evidenced by the grooves along the BSS of the MTC.

In zone 1, the compressive nature of the MTC is exhibited in the stacked nature of blocks in Zone 1. Also, the frontally emergent nature of the MTC in the zone 2 region of the study area highlights the erosive strength of the basal shear surface MTC (Martínez et al., 2006; Alsop et al., 2018; Sobiesiak et al., 2018). The erosional interaction between the MTC and the basal surface (Fig. 3) could be associated with slope changes or height drop and likely contribute to the emplacement style observed (e.g., Moernaut and De Batist, 2011) as well as disaggregation of the blocks and the formation of the basal ramp (Sobiesiak et al., 2018). The MTC becomes frontally confined Southwards away from zone 2, possibly due to the reduction in the erosive strength of the MTC and the high ramp angle of more than 60º. Moving from North to South, the MTC comprised more blocks and lesser deformed ones just before the ramp (zone 2). In zone 1 of the study area (after the ramp), the blocks are more deformed, while there are fewer blocks and more deformations of the blocks in zone 3 (not associated with the ramp).

Additional factors like the slope angle variation of the detach-ment surface (BSS) played a vital role in ramp development and sub-sequent block deformation. When the basal shear surface ramps up, it forms uneven bedding planes, and the sediments that eventually translate over the ramp usually experience significant deformation (Alsop et al., 2022). The ramp interpreted in the study area can be de-scribed as a promontory-type and fault-related ramp (Omosanya and Alves, 2013).

5.3. Implication for understanding blocks within mass transport complexes

The study has allowed for the recognition of MTCs on the present-day seafloor of the southwestern Orange Basin. The MTC has been delimited according to its morphology, dimensions, chronology, and subsequent internal filling architecture and its geometrical relationship with the surrounding host stratigraphy. Without direct chronological data from industrial boreholes or ODP wells in this area, it remains dif-ficult to establish the exact timing of the MTC events. However, It has been possible to deduce their relative chronological succession (dating to the Neogene) using cross-cutting relationships with nearby succes-sions that have been documented and published (Brown, 1995; Hirsch et al., 2007; Paton et al., 2007; Mello et al., 2012; Scarselli et al., 2016;

Dalton et al., 2017; Scarselli, 2020; Mahlalela et al., 2021). The identified geomorphological features and characteristics of the MTC (e.g., grooves, coves, striations, Basal shear surface) provided insight into the transla-tion and sediment source of the MTC and the blocks within them from the NE to the SW.

Gamboa et al. (2012) and Armandita et al. (2015) discussed the in-ternal geometry of MTCs and their implications on their source, re-mobilization, and structural emplacements. (Gamboa et al., 2012) noted that increasing block deformations indicate larger travel dis-tances. In the study area, the observed blocks were minor, moderately, and majorly deformed, indicating varying travel distances. Further-more, minor deformed blocks suggest that the blocks are either rem-nant or localized.

Furthermore, Gamboa et al. pointed out that underlying faults arrays exert some control on block geometry and deformation. In the study area, underlying faults have aided block separation (Fig. 5).

6. Conclusions

By combining seismic interpretation methods and statistical analysis of morphometric parameters, this work has provided insights into the presence of submarine blocks within a near seafloor mass transport complex, their provenance, and deformation evolution in the deepwa-ter setting of Orange Basin, offshore South Africa. The development and morphology of the MTC and the block features were influenced by the erosive nature of its basal shear surface (BSS) manifested by grooves, striations, and ramps. Based on the analysis of kinematic fea-tures like grooves and striations, the MTC is adjudged to have been transported from the NE to the SW direction.

A total of 41 blocks were identified, showing different and folded in-ternal reflections (folded and well-defined outlines, including Very elongated, very bladed, and very platy geometries). Blocks within the MTC were grouped into three zones based on block density, erosion in-tensity, and variations in deformation. Average block sizes range from 109 m to 183 m. A significant ramp (max. Height of 300 m) is located southwest of the study area. The ramp developed at the southern end of the cove-like feature and affected the deformation (slightly, moder-ately, and major deformations) and distribution of blocks.

Limited data did not permit a detailed study of the provenance of the blocks and prevented us from making a definite chronological classifica-tion of the MTC and blocks identified in the study area. Future research will focus on detailed chronological classification and provenance anal-ysis of the MTC.

CRediT authorship contribution statement

The authors confirm the contribution to the paper as follows: Study conception and design: POA, MO; Interpretation and Analysis: POA; Draft and Manuscript preparation: POA. All authors reviewed the results and approved the final version of the manuscript.

Data availability

The datasets used in this study are available from the corresponding author upon reasonable request.

Declaration of competing interest

The authors declare that they have no known competing financial interests or personal relationships that could have appeared to influ-ence the work reported in this paper.

Acknowledgements

Cape used in this research. We acknowledge Schlumberger for granting the University of Western Cape and the University of Haifa academic licenses of Petrel used in the study. POA thanks the Graduate Studies Authority at the University of Haifa for a one-year fellowship granted to visit Petrolab and the Applied Marine Exploration Lab (AMEL) for hosting POA and carrying out part of the analyses presented in this work. And we also thank the reviewers who painstakingly reviewed this work. The authors also acknowledge the contributions of Dr. Kamaldeen Olakunle Omosanya and Dr. Ovie Emmanuel Eruteya in preparing Figs. 2, 5, and 7.

References

Alsop, G.I., Weinberger, R., Marco, S., 2018. Distinguishing thrust sequences in gravity-driven fold and thrust belts. Journal of Structural Geology 109 (June 2017), 99–119. https://doi.org/10.1016/j.jsg.2018.01.005.

Alsop, G.I., Marco, S., Levi, T., 2022. Recognizing surface versus sub-surface deformation of soft sediments: Consequences and considerations for palaeoseismic studies. Journal of Structural Geology 154. https://doi.org/10.1016/j.jsg.2021.104493.

Alves, T.M., 2015. Submarine slide blocks and associated soft-sediment deformation in deepwater basins: a review. Marine and Petroleum Geology 67, 262–285. https://doi.org/10.1016/j.marpetgeo.2015.05.010.

Alves, T.M., Cartwright, J.A., 2010. The effect of mass-transport deposits on the younger slope morphology, offshore Brazil. Marine and Petroleum Geology 27, 2027–2036. https://doi.org/10.1016/j.marpetgeo.2010.05.006.

Armandita, C., Morley, C.K., Rowell, P., 2015. Origin, structural geometry, and development of a giant coherent slide: the South Makassar Strait mass transport complex. Geosphere 11, 376–403. https://doi.org/10.1130/GES01077.1.

Artoni, A., Polonia, A., Carlini, M., Torelli, L., Mussoni, P., Gasperini, L., 2019. Mass Transport Deposits and geohazard assessment in the Bradano Foredeep (Southern Apennines, Ionian Sea). Marine Geology 407, 275–298. https://doi.org/10.1016/j.margeo.2018.11.008.

Belousov, A., Belousova, M., Voight, B., Belousov, Alexander, Belousova, Marina, Voight, Barry, 1999. Multiple Edifice Failures, Debris Avalanches and Associated Eruptions in the Holocene History of Shiveluch Volcano, Kamchatka, Russia. Springer-Verlag.

Bhattacharya, S., Verma, S., Rotzien, J., 2020. 3D seismic imaging of the submarine slide blocks on the north slope, Alaska. Interpretation 8. https://doi.org/10.1190/int-2020-0038.1.

Brown, L.F., 1995. Sequence Stratigraphy in Offshore South African Divergent Basins: an Atlas of Exploration for Cretaceous Lowstand Traps by Soekor (Pty) Ltd. Sequence stratigraphy in offshore South African divergent basins: an atlas of exploration for Cretaceous lowstand traps by Soekor (Pty) Ltd.

Bull, S., Cartwright, J., Huuse, M., 2009. A review of kinematic indicators from mass-transport complexes using 3D seismic data. Marine and Petroleum Geology 26, 1132–1151. https://doi.org/10.1016/j.marpetgeo.2008.09.011.

Burgess, P.M., Hovius, N., 1998. Rates of delta progradation during highstands: Consequences for timing of deposition in deep-marine systems. Journal of the Geological Society 155, 217–222. https://doi.org/10.1144/gsjgs.155.2.0217.

Carvajal, C., Steel, R., Petter, A., 2009. Sediment supply: the main driver of shelf-margin growth. Earth-Science Reviews 96, 221–248.

Chopra, S., Marfurt, K., 2008. Gleaning meaningful information from seismic attributes. First Break 26, 43–53.

Cossey, S.P.J., 2011. Mass-transport deposits in the Upper Paleocene Chicontepec Formation, Mexico. Mass-Transport Deposits in Deepwater Settings, pp. 269–277 https://doi.org/10.2110/sepmsp.096.269.

Cox, D.R., Huuse, M., Newton, A.M.W., Gannon, P., Clayburn, J., 2020. Slip sliding away: Enigma of large sandy blocks within a gas-bearing mass transport deposit, offshore northwestern Greenland. AAPG Bulletin 104, 1011–1043. https://doi.org/10.1306/10031919011.

Crespo-Blanc, A., Campos, J., 2001. Structure and kinematics of the South Iberian paleomargin and its relationship with the Flysch Trough units: Extensional tectonics within the Gibraltar Arc fold-and-thrust belt (western Betics). Journal of Structural Geology 23, 1615–1630. https://doi.org/10.1016/S0191-8141(01)00012-8.

Dalton, T.J.S., Paton, D.A., Needham, D.T., 2017. Influence of mechanical stratigraphy on multi-layer gravity collapse structures: Insights from the Orange Basin, South Africa. Geological Society Special Publication 438, 211–228. https://doi.org/10.1144/SP438.4.

Davis, G.H., Phillips, M.P., Reynolds, S.J., Varga, R.J., 1979. Origin and provenance of some exotic blocks in lower Mesozoic red-bed basin deposits, southern Arizona. Bulletin of the Geological Society of America 90, 376–384. https://doi.org/10.1130/0016-7606(1979)90<376:OAPOSE>2.0.CO;2.

De Blasio, F.V., Engvik, L.E., Elverhøi, A., 2006. Sliding of outrunner blocks from submarine landslides. Geophysical Research Letters 33, L06614. https://doi.org/10.1029/2005GL025165.

De Vera, J., Granado, P., McClay, K., 2010. Structural evolution of the Orange Basin gravity-driven system, offshore Namibia. Marine and Petroleum Geology 27, 223–237.

Deckers, J., 2015. Middle Miocene mass transport deposits in the southern part of the Roer Valley Graben. Marine and Petroleum Geology 66, 653–659. https://doi.org/10.1016/j.marpetgeo.2015.07.006.

Deptuck, M., Mosher, D.C., Campbell, D.C., Hughes-Clarke, J.E., Noseworthy, D., 2007. Along slope variations in mass failures and relationships to major plio-pleistocene morphological elements, SW Labrador Sea. In: Lykousis, V., Sakellariou, D., Locat, J.

(Eds.), Submarine Mass Movements and Their Consequences: 3 International Symposium, Advances in Natural and Technological Hazards Research. Springer, Netherlands, Dordrecht, pp. 37–47.

DeVore, J.R., Sawyer, D.E., 2016. Shear strength of siliciclastic sediments from passive and active margins (0–100 m below seafloor): insights into seismic strengthening. Submarine Mass Movements and their Consequences. Springer, pp. 173–180.

Dott Jr., R.H., 1963. Dynamics of subaqueous gravity depositional processes. AAPG Bulletin 47, 104–128.

Doughty-Jones, G., Lonergan, L., Mayall, M., Dee, S.J., 2019. The role of structural growth in controlling the facies and distribution of mass transport deposits in a deepwater salt minibasin. Marine and Petroleum Geology 104, 106–124. https://doi.org/10.1016/j.marpetgeo.2019.03.015.

Gamboa, D., Alves, T., Cartwright, J., 2011. Distribution and characterization of failed (mega)blocks along salt ridges, southeast Brazil: implications for vertical fluid flow on continental margins. Journal of Geophysical Research: Solid Earth 116, 1–20. https://doi.org/10.1029/2011JB008357.

Gamboa, D., Alves, T.M., Cartwright, J., 2012. Submarine Mass Movements and Their Consequences. Submarine Mass Movements and Their Consequences, pp. 629–638 https://doi.org/10.1007/978-94-007-2162-3.

Gamboa, D., Alves, T.M., Omosanya, K.O., 2020. Style and morphometry of mass-transport deposits across the espírito santo basin (Offshore SE Brazil). Geophysical Monograph Series 246, 227–246. https://doi.org/10.1002/9781119500513.ch14.

Garziglia, S., Migeon, S., Ducassou, E., Loncke, L., Mascle, J., 2008. Mass-transport deposits on the Rosetta province (NW Nile deep-sea turbidite system, Egyptian margin): Characteristics, distribution, and potential causal processes. Marine Geology 250, 180–198. https://doi.org/10.1016/j.margeo.2008.01.016.

Gawthorpe, R.L., Clemmey, H., 1985. The geometry of submarine slides in the Bowland Basin (Dinantian) and their relation to debris flows. Journal - Geological Society (London) 142, 555–565. https://doi.org/10.1144/gsjgs.142.3.0555.

Gee, M.J.R., Masson, D.G., Watts, A.B., Mitchell, N.C., 2001. Passage of debris flows and turbidity currents through a topographic constriction: seafloor erosion and deflection of flow pathways. Sedimentology 48, 1389–1409. https://doi.org/10.1046/J.1365-3091.2001.00427.X.

Gee, M.J.R., Gawthorpe, R.L., Friedmann, S.J., 2006. Triggering and evolution of a giant submarine landslide, Offshore Angola, Revealed by 3D seismic stratigraphy and geomorphology. Journal of Sedimentary Research 76, 9–19. https://doi.org/10.2110/jsr.2006.02.

Giles, M.K., Mosher, D.C., Piper, D.J.W., Wach, G.D., 2010. Mass transport deposits on the southwestern newfoundland slope. In: Mosher, David C., Shipp, R.C., Moscardelli, L., Chaytor, J.D., Baxter, C.D.P., Lee, H.J., Urgeles, R. (Eds.), Submarine Mass Movements and Their Consequences, Advances in Natural and Technological Hazards Research. Springer Netherlands, Dordrecht, pp. 657–665 https://doi.org/10.1007/978-90-481-3071-9_53.

Goodbred, S.L., Kuehl, S.A., 2000. The significance of large sediment supply, active tectonism, and eustasy on margin sequence development: Late Quaternary stratigraphy and evolution of the Ganges-Brahmaputra delta. Sedimentary Geology 133, 227–248. https://doi.org/10.1016/S0037-0738(00)00041-5.

Graham, D.J., Midgley, N.G., 2000. Graphical representation of particle shape using triangular diagrams: an excel spreadsheet method. Earth Surface Processes and Landforms 25, 1473–1477. https://doi.org/10.1002/1096-9837(200012)25:13<1473::AID-ESP158>3.0.CO;2-C.

Hartwig, A., Anka, Z., di Primio, R., 2012. Evidence of a widespread paleo-pockmarked field in the Orange Basin: an indication of an early Eocene massive fluid escape event offshore South Africa. Marine Geology 332–334, 222–234. https://doi.org/10.1016/j.margeo.2012.07.012.

Haughton, P., Davis, C., McCaffrey, W., Barker, S., 2009. Hybrid sediment gravity flow deposits - classification, origin and significance. Marine and Petroleum Geology 26, 1900–1918. https://doi.org/10.1016/j.marpetgeo.2009.02.012.

Hirsch, K.K., Scheck-Wenderoth, M., Paton, D.A., Bauer, K., 2007. Crustal structure beneath the Orange Basin, South Africa. South African Journal of Geology 110, 249–260. https://doi.org/10.2113/gssajg.110.2-3.249.

Hirsch, K.K., Scheck-Wenderoth, M., van Wees, J.D., Kuhlmann, G., Paton, D.A., 2010. Tectonic subsidence history and thermal evolution of the Orange Basin. Marine and Petroleum Geology 27, 565–584. https://doi.org/10.1016/j.marpetgeo.2009.06.009.

Hodgson, D.M., Brooks, H.L., Ortiz-Karpf, A., Spychala, Y., Lee, D.R., Jackson, C.A.L., 2018. Entrainment and abrasion of megaclasts during submarine landsliding and their impact on flow behaviour. 8th International Symposium on Submarine Mass Movements and Their Consequences. 2018. ISSMMTC, pp. 223–240. https://doi.org/10.1144/SP477.26.

Isiaka, A.I., Durrheim, R.J., Manzi, M.S.D., Andreoli, M.A.G., 2017. 3D seismic analysis of the AK Fault, Orange Basin, South Africa: implications for hydrocarbon leakage and offshore neotectonics. Tectonophysics 721, 477–490. https://doi.org/10.1016/j.tecto.2017.10.011.

Jia, H., Zi, F., Yang, G., Li, G., Shen, Y., Sun, Q., Yang, P., 2020. Influence of pore water (ice) content on the strength and deformability of frozen argillaceous siltstone. Rock Mechanics and Rock Engineering 53, 967–974. https://doi.org/10.1007/S00603-019-01943-0.

Jungslager, E.H.A., 1999. Petroleum habitats of the Atlantic margin of South Africa. Geological Society, London, Special Publications 153, 153–168. https://doi.org/10.1144/GSL.SP.1999.153.01.10.

Koiter, A.J., Owens, P.N., Petticrew, E.L., Lobb, D.A., 2013. The behavioural characteristics of sediment properties and their implications for sediment fingerprinting as an approach for identifying sediment sources in river basins. Earth-Science Reviews 125, 24–42.

Koson, S., Chenrai, P., Choowong, M., 2014. Bulletin of Earth Sciences of Thailand seismic attributes and their applications in seismic geomorphology. Bulletin of Earth Sciences of Thailand 6, 1–9.

Kuhlmann, G., Adams, S., Campher, C., van der Spuy, D., di Primio, R., Horsfield, B., 2010. Passive margin evolution and its controls on natural gas leakage in the southern Orange Basin, blocks 3/4, offshore South Africa. Marine and Petroleum Geology 27, 973–992. https://doi.org/10.1016/j.marpetgeo.2010.01.010.

Kumar, P.C., Omosanya, K.O., Eruteya, O.E., Sain, K., 2021. Geomorphological characterization of basal flow markers during recurrent mass movement: a case study from the Taranaki Basin, offshore New Zealand. Basin Research 33, 2358–2382. https://doi.org/10.1111/bre.12560.

Locat, J., Ten Brink, U.S., Chaytor, J.D., 2010. The block composite submarine landslide, Southern New England Slope, USA: a morphological analysis. Submarine Mass Movements and their Consequences - 4th International Symposium. Kluwer Academic Publishers, pp. 267–277 https://doi.org/10.1007/978-90-481-3071-9_22.

Lucente, C.C., Pini, G.A., 2003. Anatomy and emplacement mechanism of a large submarine slide within a Miocene foredeep in the Northern Apennines, Italy: a field perspective. American Journal of Science 303, 565–602. https://doi.org/10.2475/ajs.303.7.565.

Mahlalela, V., Manzi, M.S.D., Jinnah, Z., Bourdeau, J.E., Durrheim, R.J., 2021. Structural characteristics and 3D seismic detection of gas migration pathways in the deepwater Orange Basin, South Africa. Marine Geophysical Research 42, 8. https://doi.org/10.1007/s11001-021-09428-y.

Martinez, J.F., Cartwright, J., Hall, B., 2005. 3D seismic interpretation of slump complexes: examples from the continental margin of Israel. Basin Research 17, 83–108. https://doi.org/10.1111/j.1365-2117.2005.00255.x.

Martínez, J.F., Cartwright, J., James, D., 2006. Frontally confined versus frontally emergent submarine landslides: a 3D seismic characterization. Marine and Petroleum Geology 23, 585–604. https://doi.org/10.1016/j.marpetgeo.2006.04.002.

Masson, D.G., Harbitz, C.B., Wynn, R.B., Pedersen, G., Løvholt, F., 2006. Submarine landslides: processes, triggers, and hazard prediction. Philosophical Transactions of the Royal Society A: Mathematical, Physical and Engineering Sciences 364, 2009–2039. https://doi.org/10.1098/rsta.2006.1810.

Mello, M.R., Azambuja, N., Mohriak, We, Catto, A., Francoli, J., 2012. Promising giant new hydrocarbon frontier: the Namibian continental margin. GeoExpro 8, 1–12.

Moernaut, J., De Batist, M., 2011. Frontal emplacement and mobility of sublacustrine landslides: results from morphometric and seismostratigraphic analysis. Marine Geology 285, 29–45. https://doi.org/10.1016/j.margeo.2011.05.001.

Moore, G.F., Strasser, M., 2016. Large mass transport deposits in Kumano basin, Nankai Trough, Japan. Adv. Nat. Technol. Hazards Res. 41, 371–379. https://doi.org/10.1007/978-3-319-20979-1_37.

Moscardelli, L., Wood, L., 2008. New classification system for mass transport complexes in offshore Trinidad. Basin Research 20, 73–98. https://doi.org/10.1111/j.1365-2117.2007.00340.x.

Moscardelli, L., Wood, L., Mann, P., 2006. Mass-transport complexes and associated processes in the offshore area of Trinidad and Venezuela. AAPG Bulletin 90, 1059–1088. https://doi.org/10.1306/02210605052.

Mosher, D.C., Campbell, D.C., Gardner, J.V., Piper, D.J.W., Chaytor, J.D., Rebesco, M., 2017. The role of deepwater sedimentary processes in shaping a continental margin: the Northwest Atlantic. Marine Geology 393, 245–259. https://doi.org/10.1016/j.margeo.2017.08.018.

Muntingh, A., Brown Jr., L.F., 1993. Sequence stratigraphy of petroleum plays, post-rift Cretaceous rocks (Lower Aptian to Upper Maastrichtian), Orange Basin, Western Offshore, South Africa. AAPG Memoir 58: Siliciclastic Sequence Stratigraphy: Recent Developments and Applications, pp. 71–98.

Ngeri, A.P., Tamunobereton-ari, I., Amakiri, A.R.C., 2015. Ant-tracker attributes: an effective approach to enhancing fault identification and interpretation. Journal of VLSI and Signal Processing 5, 67–73. https://doi.org/10.9790/4200-05626773.

Nissen, S.E., Haskell, N.L, Steiner, C.T., Coterill, K.L., 1999. Debris flow outrunner blocks, glide tracks, and pressure ridges identified on the Nigerian continental slope using 3-D seismic coherency. The Leading Edge 18, 595–599. https://doi.org/10.1190/1.1438343.

Nugraha, H.D., Jackson, C.A.-L., Johnson, H.D., Hodgson, D.M., 2020. Lateral variability in strain along the toewall of a mass transport deposit: a case study from the Makassar Strait, offshore Indonesia. Journal of the Geological Society 177, 1261–1279. https://doi.org/10.1144/jgs2020-071.

Nwoko, J., Kane, I., Huuse, M., 2020. Megaclasts within mass-transport deposits: their origin, characteristics and effect on substrates and succeeding flows. Geological Society Special Publication. Geological Society of London, pp. 515–530 https://doi.org/10.1144/SP500-2019-146.

Ogiesoba, O., Hammes, U., 2012. Seismic interpretation of mass-transport deposits within the upper Oligocene Frio Formation, south Texas Gulf Coast. AAPG Bulletin 96, 845–868. https://doi.org/10.1306/09191110205.

Omosanya, K.O., Alves, T.M., 2013. Ramps and flats of mass-transport deposits (MTDs) as markers of seafloor strain on the flanks of rising diapirs (Espírito Santo Basin, SE Brazil). Marine Geology 340, 82–97. https://doi.org/10.1016/j.margeo.2013.04.013.

Omosanya, K.O., Maia, A.R., Eruteya, O.E., 2020. Seismic, morphologic and scale variabilities of subsurface pipes and vent complexes in a magma-rich margin. Bulletin of Volcanology 82. https://doi.org/10.1007/s00445-020-01379-3.

Paton, D.A., di Primio, R., Kuhlmann, G., van der Spuy, D., Horsfield, B., 2007. Insights into the Petroleum System Evolution of the southern Orange Basin, South Africa. South African Journal of Geology 110, 261–274. https://doi.org/10.2113/gssajg.110.2-3.261.

Peel, F.J., 2014. The engines of gravity-driven movement on passive margins: quantifying the relative contribution of spreading vs. gravity sliding mechanisms. Tectonophysics 633, 126–142. https://doi.org/10.1016/j.tecto.2014.06.023.

Petroleum Agency of SA, 2008. Republic of South Africa Petroleum Exploration Potential of the Orange Basin Regional Geology.

Pickering, K.T., Corregidor, J., 2005. Mass-Transport Complexes (MTCs) and Tectonic Control on Basin-Floor Submarine fans, Middle Eocene, South Spanish Pyrenees. Journal of Sedimentary Research 75, 761–783. https://doi.org/10.2110/jsr.2005.062.

Prather, B.E., Booth, J.R., Steffens, G.S., Craig, P.A., 1998. Succession of seismic facies of intraslope basins, Deep-Water Gulf of Mexico I. AAPG Bulletin 82, 701–728. https://doi.org/10.1306/1D9BC5D9-172D-11D7-8645000102C1865D.

Prior, D.B., Bornhold, B.D., Johns, M.W., 1984. Depositional characteristics of a submarine debris flow. Journal of Geology 92, 707–727. https://doi.org/10.1086/628907.

Rusconi, F.J., 2017. 3D Seismic Interpretation of a Plio-Pleistocene Mass Transport Deposit in the Deepwater Taranaki Basin of New Zealand. p. 57.

Samakinde, C.A., van Bever Donker, J.M., Durrheim, R., Manzi, M., 2021. Hydrocarbon generation and migration from Barremian – Aptian source rocks, northern orange basin, offshore western south Africa: a 3d numerical modelling study. Journal of Petroleum Geology 44, 187–208. https://doi.org/10.1111/jpg.12785.

Scarselli, N., 2020. Submarine landslides – Architecture, controlling factors and environments. A summary. In: Scarselli, N., Adam, J., Chiarella, D., Roberts, D.G., Bally, A.W. (Eds.), Regional Geology and Tectonics, Second edition Elsevier, pp. 417–439 https://doi.org/10.1016/b978-0-444-64134-2.00015-8.

Scarselli, N., McClay, K., Elders, C., 2016. Seismic geomorphology of cretaceous megaslides offshore Namibia (Orange Basin): insights into segmentation and degradation of gravity-driven linked systems. Marine and Petroleum Geology 75, 151–180. https://doi.org/10.1016/j.marpetgeo.2016.03.012.

Shanmugam, G., 2013. New perspectives on deepwater sandstones: implications. Petroleum Exploration and Development 40, 316–324.

Shanmugam, G., 2015. The landslide problem. Journal of Palaeogeography 2015, 109–166. https://doi.org/10.3724/SP.J.1261.2015.00071.

Shipp, R.C., Weimer, P., Posamentier, H.W., Shipp, R.C., Weimer, P., Posamentier, H.W., 2015. Mass-Transport Deposits in Deepwater Settings. Mass-Transport Deposits in Deepwater Settings. https://doi.org/10.2110/sepmsp.096.

Sneed, E.D., Folk, R.L., 1958. Pebbles in the Lower Colorado River, Texas a Study in Particle Morphogenesis. The Journal of Geology 66, 114–150. https://doi.org/10.1086/626490.

Sobiesiak, M.S., Kneller, B., Ian Alsop, G., Milana, J.P., 2016. Inclusion of substrate blocks within a mass transport deposit: a case study from Cerro Bola, Argentina. Advances in Natural and Technological Hazards Research, pp. 487–496 https://doi.org/10.1007/978-3-319-20979-1_49.

Sobiesiak, M.S., Kneller, B., Alsop, G.I., Milana, J.P., 2018. Styles of basal interaction beneath mass transport deposits. Marine and Petroleum Geology 98, 629–639. https://doi.org/10.1016/j.marpetgeo.2018.08.028.

Sobiesiak, M.S., Buso, V.V., Kneller, B., Alsop, G.I., Milana, J.P., 2020. Block generation, deformation, and interaction of mass-transport deposits with the seafloor: an outcrop-based study of the carboniferous Paganzo Basin (Cerro Bola, NW Argentina). Geophysical Monograph Series 246, 91–104. https://doi.org/10.1002/9781119500513.ch6.

Steventon, M.J., Jackson, C.A., Hodgson, D.M., Johnson, H.D., 2019. Strain analysis of a seismically imaged mass-transport complex, offshore Uruguay. Basin Research 31, 600–620. https://doi.org/10.1111/bre.12337.

Strachan, L.J., 2002. Slump-initiated and controlled syndepositional sandstone remobilization: an example from the Namurian of county Clare, Ireland. Sedimentology 49, 25–41. https://doi.org/10.1046/j.1365-3091.2002.00430.x.

Strasser, M., Moore, G.F., Kimura, G., Kopf, A.J., Underwood, M.B., Guo, J., Screaton, E.J., 2012. Slumping and mass transport deposition in the Nankai fore arc: evidence from IODP drilling and 3-D reflection seismic data. Geochemistry, Geophysics, Geosystems 12, 1–24. https://doi.org/10.1029/2010GC003431.

Trincardi, F., Argnani, A., 1990. Gela submarine slide: a major basin-wide event in the plio-quaternary foredeep of Sicily. Geo-Marine Letters 10, 13–21. https://doi.org/10.1007/BF02431017.

Urgeles, R., Camerlenghi, A., 2013. Submarine landslides of the Mediterranean Sea: trigger mechanisms, dynamics, and frequency-magnitude distribution. Journal of Geophysical Research: Earth Surface 118, 2600–2618. https://doi.org/10.1002/2013JF002720.

Urlaub, M., Talling, P.J., Masson, D.G., 2013. Timing and frequency of large submarine landslides: implications for understanding triggers and future geohazard. Quaternary Science Reviews 72, 63–82. https://doi.org/10.1016/J.QUASCIREV.2013.04.020.

Vanneste, M., Forsberg, C.F., Glimsdal, S., Harbitz, C.B., Issler, D., Kvalstad, T.J., Løvholt, F., Nadim, F., 2013. Submarine landslides and their consequences: what do we know, what can we do? Landslide Science and Practice. Springer, pp. 5–17

Ward, N.I.P., Alves, T.M., Blenkinsop, T.G., 2018. Submarine sediment routing over a blocky mass-transport deposit in the Espírito Santo Basin, SE Brazil. Basin Research 30, 816–834. https://doi.org/10.1111/bre.12282.

Wendorff, M., 2003. Stratigraphy of the Fungurume Group - evolving foreland basin succession in the Lufilian fold-thrust belt, Neoproterozoic-lower Paleozoic, Democratic Republic of Congo. South African Journal of Geology 106, 17–34. https://doi.org/10.2113/1060017.

Wu, N., Jackson, C.A.L., Johnson, H.D., Hodgson, D.M., Clare, M.A., Nugraha, H.D., Li, W., 2021. The formation and implications of giant blocks and fluid escape structures in submarine lateral spreads. Basin Research 33, 1711–1730. https://doi.org/10.1111/bre.12532.

Zitter, T.A.C., Grall, C., Henry, P., Özeren, M.S., Çağatay, M.N., Şengör, A.M.C., Gasperini, L., de Lépinay, B.M., Géli, L., 2012. Distribution, morphology, and triggers of submarine mass wasting in the Sea of Marmara. Marine Geology 329–331, 58–74. https://doi.org/10.1016/j.margeo.2012.09.002.